INTERNATIONAL JOURNAL FOR NUMERICAL METHODS IN FLUIDS
Int. J. Numer. Meth. Fluids 2008; **58**:427–449
Published online 18 February 2008 in Wiley InterScience (www.interscience.wiley.com). DOI: 10.1002/fld.1751

A fast and robust fictitious domain method for modelling viscous flows in complex mixers: The example of propellant make-down

Benjamin Coesnon[1,2], Mourad Heniche[1,2], Christophe Devals[1,2], François Bertrand[1,2,*,†] and Philippe A. Tanguy[1,2]

[1]*Research Unit for Industrial Flows Processes* (*URPEI*), *Department of Chemical Engineering*, *Ecole Polytechnique de Montreal*, *P.O. Box 6079*, *Stn. Centre-Ville*, *Montreal*, *Que.*, *Canada H3C 3A7*
[2]*Center for Applied Research on Polymers and Composites* (*CREPEC*), *Department of Chemical Engineering*, *Ecole Polytechnique de Montreal*, *P.O. Box 6079*, *Stn. Centre-Ville*, *Montreal*, *Que.*, *Canada H3C 3A7*

SUMMARY

This work deals with the development of a fast three-dimensional numerical strategy for the simulation of viscous fluid flow in complex mixing systems. The proposed method is based on a distributed Lagrange multiplier fictitious domain method and the use of the low-cost MINI finite element. Contrary to the previous fictitious domain method developed by our group a few years ago, the underlying partial differential equations are solved here in a coupled manner using a consistent penalty technique. The method is discussed in detail and its precision is assessed by means of experimental data in the case of an agitated vessel. A comparison made with our existing fictitious domain method and its decoupled Uzawa-based solver clearly shows the advantages of resorting to the MINI finite element and fully coupled solution strategy. The new technique is then applied to the simulation of the flow of a Newtonian viscous fluid in a three-blade planetary mixer in the context of the production of solid propellants. Copyright © 2008 John Wiley & Sons, Ltd.

Received 17 August 2007; Revised 12 December 2007; Accepted 16 December 2007

KEY WORDS: fictitious domain method; finite element method; MINI element; laminar; Maxblend mixer; planetary mixer

*Correspondence to: François Bertrand, Center for Applied Research on Polymers and Composites (CREPEC), Department of Chemical Engineering, Ecole Polytechnique de Montreal, P.O. Box 6079, Stn. Centre-ville, Montreal, Que., Canada H3C 3A7.
†E-mail: francois.bertrand@polymtl.ca

Contract/grant sponsor: National Science and Engineering Research Council of Canada (NSERC)
Contract/grant sponsor: Fond Québecois de la Recherche sur la Nature et les Technologies (FQRNT)

1. INTRODUCTION

The mixing of very viscous fluids in mechanically agitated vessels is a common operation in numerous industries. One example is the mixing of very fine solids at high loading rates in a viscous polymeric matrix, which finds applications in the production of propellant pastes for aerospace and automobile industries. These materials are prepared through fabrication cycles that are complex, costly and time consuming. As discussed in Tanguy *et al.* [1], the manufacturing line is subjected to the following two central difficulties:

- the fluid is paste-like and highly viscous. Hence, the mixing is achieved in laminar regime;
- small quantities in the formulation must be thoroughly distributed and dispersed to yield the right mechanical and combustion properties.

The operation of blending very viscous pastes may be achieved by four different mixing systems: vertical planetary kneaders, horizontal multiple impeller kneaders, helical ribbon impellers and twin-screw extruders. Since the mid-1960s, solid rocket propellant mixing has been often carried out through vertical planetary mixers.

The analysis of mixer performance can be done through the evaluation of macroscopic quantities such as mixing time or power draw. Evaluating these quantities experimentally is a time-consuming and expensive task. Three-dimensional computational fluid dynamics (CFD) simulation then appears as a useful alternative for the investigation of a mixing process. However, the biggest challenge for the modelling of mixing with a planetary mixer such as the three-blade planetary kneader is that the geometry contains moving parts with complex kinematics, which entails the generation of a new mesh at every time iteration when using standard CFD (finite element or finite volume) techniques.

In the literature, several numerical simulation techniques within the finite element method framework have been proposed to eliminate the need for repetitive remeshings.

Bertrand *et al.* [2] introduced the virtual finite element method (VFEM), a fictitious domain method that is based on optimization techniques as first proposed by Glowinski *et al.* [3]. In the context of fluid flow in agitated tanks, the internal blades are discretized using control points on which kinematics constraints are imposed and introduced in the equations of change by means of Lagrange multipliers. Bertrand *et al*. [4] and Tanguy *et al.* [1, 5–7] used the VFEM technique to simulate mixing flows in a twin-blade planetary mixer. Each time, the numerical results were in very good agreement with experimental data.

Jongen [8] and Jongen *et al.* [9] used a modified version of the VFEM implemented in FIDAP (ANSYS) for characterizing mixing flows in various batch mixers, one of which was a planetary mixer. More particularly, they studied the influence of mixer configurations and operating conditions on the shear rate exerted on viscous pastes.

Avalosse and Crochet [10] proposed the so-called mesh superposition technique (MST). In this method, a static mesh representing the motionless part of the flow domain and one additional dynamic mesh are superimposed at every time step of a transient simulation. The velocity of these moving parts is taken into account in the equations of change by a penalty formulation. This method has been used in Polyflow (ANSYS) to model the flow of a viscous fluid in a twin-screw extruder in two dimensions [10] and in three dimensions [11]. More recently, Connelly and Kokini [12] used the MST to simulate the three-dimensional flow of a viscous fluid in a sigma blade mixer.

DOI: 10.1002/fld

More recently, Gartling [13] extended the sliding mesh (SM) technique within a finite element framework to take into account moving objects in the computational domain by the recourse to a penalty technique. He showed the effectiveness of the method by simulating fluid flow in a rotating three-blade impeller system.

Also of interest is the work of Clifford *et al.* [14] who investigated experimentally the effect of the Reynolds number on a planetary mixer. Finally, Delaplace *et al.* [15, 16] presented a dimensional analysis for the flow in a TRIAXE® system consisting of a pitched blade turbine mounted on two almost perpendicular rotational axes.

Except for the SM technique, all the methods mentioned above belong to the class of fictitious domain methods and are well adapted to the treatment of complex geometries with evolving topologies. They are, however, rather time consuming, in particular if they are to be used for industrial applications.

The objective of this paper is to introduce a variant of the VFEM that we introduced a few years ago [2], and to show that it is both fast and robust for the simulation of viscous fluid flow in complex mixing systems such as the planetary mixers. This distributed Lagrange multiplier fictitious domain method is based on the use of the inexpensive MINI finite element and, contrary to our previous fictitious domain method (VFEM) and its decoupled Uzawa solver, it resorts to a consistent penalty technique for solving the underlying partial differential in a coupled manner.

First, the method is presented in detail. Next, its precision is assessed by means of experimental data that were obtained in the case of a Maxblend mixer, with and without baffles. A comparison is also made with our existing VFEM. Finally, our new technique is applied to the simulation of the flow of a Newtonian viscous fluid, typical of a solid propellant, in an industrial three-blade planetary mixer. The solutions obtained are all discussed in terms of both accuracy and CPU time.

2. EQUATIONS OF CHANGE

The flow of an incompressible viscous flow in a computational domain Ω with boundary Γ containing a moving part Ω^*, as presented in Figure 1, is governed by the momentum and continuity equations:

$$\rho\left(\frac{\partial \mathbf{v}}{\partial t}+\mathbf{v}\cdot\operatorname{grad}\mathbf{v}\right)+\operatorname{div}\tau+\operatorname{grad}p=\mathbf{f}\quad\text{in }\Omega \tag{1}$$

$$\operatorname{div}\mathbf{v}=0\quad\text{in }\Omega \tag{2}$$

$$\mathbf{v}=\mathbf{v}^*\quad\text{on }\Gamma^* \tag{3}$$

where Γ^* is the boundary of Ω^* and where (3) can be viewed as a kinematic constraint to be satisfied by the solution.

In these equations, $\mathbf{v}$ is the velocity, $\mathbf{v}^*$ the prescribed velocity on the moving part, $\mathbf{f}$ a body force, p the pressure and ρ the fluid density. The stress tensor τ is a function of the rate-of-strain tensor $\dot{\gamma}$, as expressed by a rheological equation of state:

$$\tau=-2\eta(|\dot{\gamma}|)\dot{\gamma} \tag{4}$$

DOI: 10.1002/fld

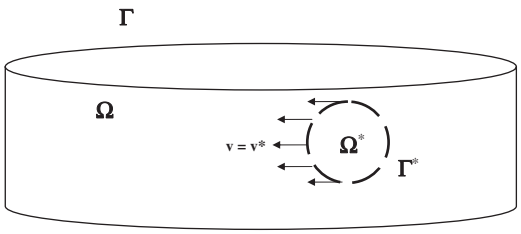

Figure 1. Computational domain Ω with an internal part Ω^* of boundary Γ^*.

with

$$\dot{\gamma} = \tfrac{1}{2}[\operatorname{grad}\mathbf{v} + (\operatorname{grad}\mathbf{v})^{\mathrm{T}}] \tag{5}$$

In this work, the Newtonian model is considered, $\eta(|\dot{\gamma}|) = \mu$, and (1) becomes the Navier–Stokes equation:

$$\rho\left(\frac{\partial \mathbf{v}}{\partial t} + \mathbf{v}\cdot\operatorname{grad}\mathbf{v}\right) + \mu\nabla^2\mathbf{v} + \operatorname{grad} p = \mathbf{f} \tag{6}$$

Appropriate initial conditions and boundary conditions on Γ must also be applied for mathematical well posedness.

3. NUMERICAL STRATEGY

For three-dimensional fluid flow problems involving internal moving parts, the VFEM considers the moving objects in the computational domain as a set of control points on which kinematics constraints are applied. These are then enforced in the equations of change by the use of Lagrange multipliers and constrained optimization techniques. If we first consider the application of this method to a steady-state Stokes problem (omitting the acceleration and inertia terms in (1)), the following saddle-point problem results:

$$\inf_{\mathbf{v}\in[H_0^1(\Omega)]^3} \sup_{p\in L^2(\Omega)} \sup_{\lambda\in[L^2(\Gamma^*)]^3} L_{\mathrm{rs}}^*(\mathbf{v}, p, \lambda) \tag{7}$$

where $\lambda \in [L^2(\Gamma^*)]^3$ is the Lagrange multiplier representing the kinematics conditions on the boundary Γ^* of the internal moving part and L_{rs}^* corresponds to the Lagrangian:

$$L_{\mathrm{rs}}^*(\mathbf{v}, p, \lambda) = L_r(\mathbf{v}, p) - \int_{\Gamma^*} \lambda\cdot(\mathbf{v} - \mathbf{v}^*)\,\mathrm{d}\Gamma + \frac{s}{2}\int_{\Gamma^*} |v - v^*|^2\,\mathrm{d}\Gamma \tag{8}$$

$$L_r(\mathbf{v}, p) = \frac{\mu}{2}\int_\Omega |\operatorname{grad}\mathbf{v}|^2\,\mathrm{d}\Omega - \int_\Omega p\operatorname{div}\mathbf{v}\,\mathrm{d}\Omega - \int_\Omega \mathbf{f}\cdot\mathbf{v}\,\mathrm{d}\Omega + \frac{r}{2}\int_\Omega |\operatorname{div}\mathbf{v}|^2\,\mathrm{d}\Omega \tag{9}$$

DOI: 10.1002/fld

The Euler–Lagrange equations corresponding to this problem are given by

$$a(\mathbf{v},\psi)=(\mathbf{f},\psi)+b(\psi,p)+(\lambda,\psi)_{\Gamma^*}\quad\forall\psi\in[H_0^1(\Omega)]^3 \tag{10}$$

$$b(\mathbf{v},\varphi)=0\quad\forall\varphi\in L^2(\Omega) \tag{11}$$

$$((\mathbf{v}-\mathbf{v}^*),\xi)_{\Gamma^*}=0\quad\forall\xi\in[L^2(\Gamma^*)]^3 \tag{12}$$

where

$$a(\mathbf{v},\psi)=\mu\int_\Omega \operatorname{grad}\mathbf{v}\cdot\operatorname{grad}\psi\,\mathrm{d}\Omega \tag{13}$$

$$b(\mathbf{v},\varphi)=\int_\Omega \varphi\cdot\operatorname{div}\mathbf{v}\,\mathrm{d}\Omega \tag{14}$$

and $(\cdot,\cdot)_\Omega$ is the standard scalar product in $L^2(\Omega)$:

$$(\mathbf{u},\mathbf{v})_\Omega=\int_\Omega \mathbf{u}\cdot\mathbf{v}\,\mathrm{d}\Omega\quad\forall\mathbf{u},\mathbf{v}\in L^2(\Omega) \tag{15}$$

Note that the inertia term can be added formally to (10) if needed. More details about the VFEM can be found in Bertrand *et al*. [2].

In the present work, the low-order $P_1^+-P_1$ (MINI) tetrahedral element is used to approximate the velocity $\mathbf{v}_h\in V_h$ and the pressure $p_h\in P_h$. It is a stable element owing to the addition of a bubble function that can be eliminated by static condensation to reduce CPU time [17]. The Lagrange multiplier $\lambda_h\in\Lambda_h$ is discretized using Dirac shape functions following Bertrand *et al*. [2]. The system of Equations (10)–(12) can be solved by means of different techniques.

3.1. Decoupled approach

In Bertrand *et al*. [2], Equations (10)–(12) were solved in a fully decoupled manner using the Uzawa method. To speed up the solution process, it is proposed in the current work to resort to partial decoupling, wherein the velocity and pressure are solved for in a coupled manner through a penalty technique, and the Lagrange multiplier is obtained as in Bertrand *et al*. [2] through the Uzawa algorithm. This strategy implies that (11) is replaced by

$$b(\mathbf{v}_h,\varphi_h)=-\frac{1}{\varepsilon_p}(p_h,\varphi_h)\quad\forall\varphi_h\in P_h \tag{16}$$

where ε_p, a large number, is the penalty parameter in pressure. Poor choices of ε_p can have a severe consequence on the validity of the computed solution. The choice of this parameter is submitted to limitations, as discussed in Reddy [18], Pelletier *et al*. [19] and Langtangen *et al*. [20]. In theory, the larger the value of ε_p, the closer (16) gets to the incompressibility condition but the larger the condition number of the associated matrix system and, consequently, the slower the convergence of the iterative method used to solve this matrix system. In this work, ε_p was scaled with respect to fluid viscosity and mesh size and set as large as possible while ensuring that mass is conserved in all simulations. The overall algorithm in its matrix form is given in Figure 2. The meaning of the different terms can be deduced straightforwardly from (10)–(12). $\mathbf{U},\mathbf{P}$ and $\mathbf{\Lambda}$ are vectors that represent the velocity, the pressure and the Lagrange multipliers, respectively. $\mathbf{A}$ stands for

DOI: 10.1002/fld

0. Given $\boldsymbol{U}^{(0)}$, $\boldsymbol{P}^{(0)}$ and $\boldsymbol{\Lambda}^{(0)}$.

1. For n = 0, 1, 2, …, until convergence:

1.1. Solve simultaneously for $\delta\boldsymbol{U}$ and $\delta\boldsymbol{P}$:

$$\begin{bmatrix} \boldsymbol{A} & \boldsymbol{B}^T \\ \boldsymbol{B} & \varepsilon_p^{-1}\boldsymbol{I} \end{bmatrix} \begin{Bmatrix} \delta\boldsymbol{U} \\ \delta\boldsymbol{P} \end{Bmatrix} = \begin{Bmatrix} \boldsymbol{R}_{U^{(n)}} \\ \boldsymbol{R}_{P^{(n)}} \end{Bmatrix}$$

$$\begin{Bmatrix} \boldsymbol{R}_{U^{(n)}} \\ \boldsymbol{R}_{P^{(n)}} \end{Bmatrix} = \begin{Bmatrix} \boldsymbol{F}\text{-}\boldsymbol{\Lambda}^{(n)} \\ \boldsymbol{0} \end{Bmatrix} - \begin{bmatrix} \boldsymbol{A} & \boldsymbol{B}^T \\ \boldsymbol{B} & \varepsilon_p^{-1}\boldsymbol{I} \end{bmatrix} \begin{Bmatrix} \boldsymbol{U}^{(n)} \\ \boldsymbol{P}^{(n)} \end{Bmatrix}$$

1.2. Update $\boldsymbol{U}^{(n)}$ and $\boldsymbol{P}^{(n)}$: $\begin{cases} \boldsymbol{U}^{(n+1)} = \boldsymbol{U}^{(n)} + \delta\boldsymbol{U} \\ \boldsymbol{P}^{(n+1)} = \boldsymbol{P}^{(n)} + \delta\boldsymbol{P} \end{cases}$

1.3 Solve for $\boldsymbol{\Lambda}^{(n+1)}$: $\boldsymbol{\Lambda}^{(n+1)} = \boldsymbol{\Lambda}^{(n)} + \beta\boldsymbol{H}\boldsymbol{U}^{(n+1)}$

Figure 2. Solution algorithm for the virtual finite element method and the decoupled approach.

the diffusion matrix, **B** stands for the divergence matrix and **F** accounts for the body force. **H** is related to the VFEM. Note that, in practice, the role of the loop (in n) is two-fold as it serves to converge the Lagrange multiplier but can also be used to implement a fixed-point method (or Newton's scheme) when the inertia term is added to the momentum equation (10).

This solution strategy has been used in our group to simulate fluid flow in mixing systems and a variety of impellers in a satisfactory manner [21, 22]. It appears that one limitation is that the Uzawa algorithm requires a large number of fixed point iterations to converge. This observation has provided the impetus for the development of a fully coupled solution strategy, which is introduced next.

3.2. Fully coupled approach

With the fully coupled approach method, the velocity $\mathbf{v}_h$, the pressure $\mathbf{p}_h$ and the Lagrange multiplier $\boldsymbol{\lambda}_h$ are all solved simultaneously by penalization. Accordingly, Equations (11) and (12) are replaced by

$$b(\mathbf{v}_h, \varphi_h) = -\frac{1}{\varepsilon_p}(p_h, \varphi_h) \quad \forall \varphi_h \in P_h \tag{17}$$

$$((\mathbf{v}_h - \mathbf{v}^*), \xi_h)_{\Gamma^*} = -\frac{1}{\varepsilon_\lambda}(\lambda_h, \xi_h)_{\Gamma^*} \quad \forall \xi_h \in \Lambda_h \tag{18}$$

where ε_p and ε_λ are penalty parameters. In practice, values for these parameters were set in a similar way as that in the previous sub-section. The resulting overall algorithm in its matrix form

DOI: 10.1002/fld

0. Given $\boldsymbol{U}^{(0)}$, $\boldsymbol{P}^{(0)}$ and $\boldsymbol{\Lambda}^{(0)}$.

1. For n = 0, 1, 2, …, until convergence:

1.1. Solve simultaneously for $\delta\boldsymbol{U}$, $\delta\boldsymbol{P}$ and $\delta\boldsymbol{\Lambda}$:

$$\begin{bmatrix} \boldsymbol{A} & \boldsymbol{B}^T & \boldsymbol{K}_{\Lambda U}^T \\ \boldsymbol{B} & \varepsilon_p^{-1}\boldsymbol{I} & \boldsymbol{0} \\ \boldsymbol{K}_{\Lambda U} & \boldsymbol{0} & \varepsilon_\lambda^{-1}\boldsymbol{I} \end{bmatrix} \begin{Bmatrix} \delta\boldsymbol{U} \\ \delta\boldsymbol{P} \\ \delta\Lambda \end{Bmatrix} = \begin{Bmatrix} \boldsymbol{R}_{U^{(n)}} \\ \boldsymbol{R}_{P^{(n)}} \\ \boldsymbol{R}_{\Lambda^{(n)}} \end{Bmatrix}$$

$$\begin{Bmatrix} \boldsymbol{R}_{U^{(n)}} \\ \boldsymbol{R}_{P^{(n)}} \\ \boldsymbol{R}_{\Lambda^{(n)}} \end{Bmatrix} = \begin{Bmatrix} \boldsymbol{F} \\ \boldsymbol{0} \\ \boldsymbol{K}_{\Lambda U}\boldsymbol{U}^* \end{Bmatrix} - \begin{bmatrix} \boldsymbol{A} & \boldsymbol{B}^T & \boldsymbol{K}_{\Lambda U}^T \\ \boldsymbol{B} & \varepsilon_p^{-1}\boldsymbol{I} & \boldsymbol{0} \\ \boldsymbol{K}_{\Lambda U} & \boldsymbol{0} & \varepsilon_\lambda^{-1}\boldsymbol{I} \end{bmatrix} \begin{Bmatrix} \boldsymbol{U}^{(n)} \\ \boldsymbol{P}^{(n)} \\ \Lambda^{(n)} \end{Bmatrix}$$

1.2. Update $\boldsymbol{U}^{(n)}$, $\boldsymbol{P}^{(n)}$ and $\boldsymbol{\Lambda}^{(n)}$: $\begin{cases} \boldsymbol{U}^{(n+1)} = \boldsymbol{U}^{(n)} + \delta\boldsymbol{U} \\ \boldsymbol{P}^{(n+1)} = \boldsymbol{P}^{(n)} + \delta\boldsymbol{P} \\ \boldsymbol{\Lambda}^{(n+1)} = \boldsymbol{\Lambda}^{(n)} + \delta\boldsymbol{\Lambda} \end{cases}$

Figure 3. Solution algorithm for the virtual finite element method and the fully coupled approach.

is given in Figure 3. The meaning of the different terms can be deduced easily from Equations (10)–(12). $\mathbf{U}, \mathbf{P}$ and $\mathbf{\Lambda}$ are vectors that represent the velocity, the pressure and the Lagrange multiplier, respectively. $\mathbf{A}$ stands for the diffusion matrix, $\mathbf{B}$ stands for the divergence matrix and $\mathbf{F}$ accounts for the body force. $\mathbf{K}_{\mathbf{\Lambda U}}$ is related to the VFEM. Note that, contrary to the decoupled approach, the loop (in n) is only required when the inertia term is added to the momentum equation (10) in order to implement a fixed-point method or Newton's scheme.

The two solution strategies presented in this section were implemented in finite element software POLY3D^{TM} from Rheosoft Inc. Owing to their large size, the underlying linear systems were solved using either the conjugate gradient method in the case of symmetric matrices (e.g. Stokes problem) and the Bi-CGSTAB or TFQMR methods in the case of unsymmetric matrices (e.g. Navier–Stokes problem with Newton's scheme). Incomplete factorization was used in all cases as a preconditioner.

The relative accuracy and speed of the new MINI-based VFEM is next assessed through experimental data obtained for mixing systems. Before, a quick discussion about mixing characterization is presented.

4. MIXING CHARACTERIZATION

One macroscopic quantity that is often used to characterize a mixing system is the power consumption P of the impeller, which can be calculated through an energy balance over the computational

DOI: 10.1002/fld

domain:

$$P = \int_{\Omega} \tau : \dot{\gamma} \, \mathrm{d}\Omega \tag{19}$$

In the field of mixing, it is also common to compare different impellers on the basis of dimensionless number K_p, the value of which is constant in the laminar regime. It is defined as

$$K_p = \frac{P}{\mu N^2 D^3} \tag{20}$$

where N is the impeller rotational speed and D its diameter. Introducing the Reynolds number for mixing systems

$$Re = \frac{\rho N D^2}{\mu} \tag{21}$$

the following expression for K_p can be established:

$$K_p = Re \, N_p \tag{22}$$

where

$$N_p = \frac{P}{\rho N^3 D^5} \tag{23}$$

is the dimensionless power number. In practice, K_p can be evaluated by a regression technique on a set of (Re, N_p) data points obtained experimentally or via CFD. The reader is referred to Paul *et al.* [23] for more information on mixing.

5. ACCURACY OF THE MINI-BASED VFEM

In this section, the accuracy and speed of the MINI element will be first investigated with a standard finite element method in the case of a vessel mechanically agitated with a Maxblend impeller without baffles using experimental data as well as numerical results obtained with another finite element type, the discontinuous pressure $P_1^+ - P_0$ element. Next, the performance of the new MINI-based VFEM of the previous section will be investigated by comparing the results obtained with it to experimental data and to those obtained with the $P_1^+ - P_0$ element. The reader is referred to Fradette *et al.* [24] and Iranshahi *et al.* [25] for more details about this mixing system, and to Bertrand *et al.* [26] for a description of the $P_1^+ - P_0$ element.

The Maxblend mixer (Sumitomo Heavy Industries[‡]), shown in Figure 4, is composed of a bottom paddle on which lies a grid-like structure. The paddle has been designed to generate efficient flow circulation while the role of the grid is to provide good dispersing capability in the case of the presence of a second phase. The Maxblend impeller represents an interesting alternative to close-clearance impellers. Table I summarizes the dimensions of the 190-l mixing system considered in this work.

[‡]http://www.shi.co.jp/maxblendclub/e-index.html.

DOI: 10.1002/fld

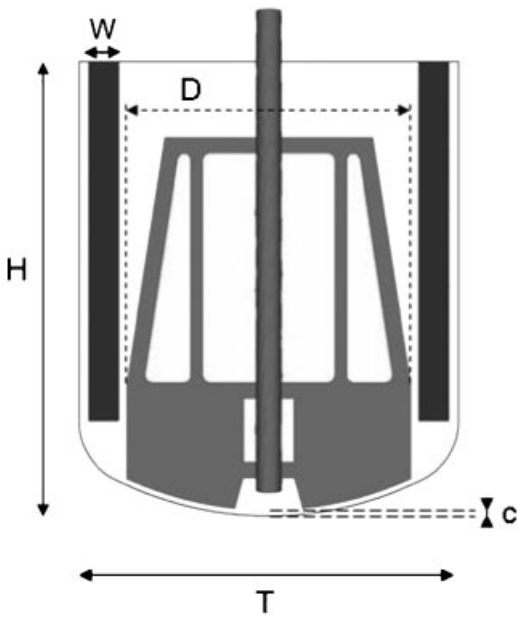

Figure 4. Schematic of the Maxblend impeller in a baffled configuration.

Table I. Dimensions of the Maxblend impeller.

Tank	Impeller	Bottom gap
$T = 0.60\,\text{m}$ $H = 0.72\,\text{m}$ $W = 0.047\,\text{m}$	$D = 0.45\,\text{m}$	$c = 10\,\text{mm}$

First, the accuracy of the MINI element is investigated with a standard finite element method. For this purpose, the Maxblend impeller system is considered in an unbaffled configuration in the case of Newtonian fluids flowing in laminar regime. For the solution of this problem, it was decided to consider the viewpoint of an observer attached to the moving impeller. As explained by Tanguy *et al*. [27], the use of this Lagrangian frame of reference makes the imposition of the boundary conditions much easier on a finite element mesh. The boundary conditions are defined by the following:

1. a no-slip condition on the impeller;
2. the rotational speed ω on the vessel walls;
3. the surface of the fluid is considered flat.

As the frame of reference is non-Galilean (the observer is in rotation with the impeller), the momentum equations must be complemented by the centrifugal and Coriolis forces. This frame of reference yields a steady-state fluid flow problem that is faster to solve than a transient one, provided the flow is fully periodic.

DOI: 10.1002/fld

For the simulations, the angular velocity ω was kept constant at 30 rpm and the Newtonian fluid had a density ρ of 1350 kg/m^3 and a viscosity μ varying from 10 to 136 Pa s, which yields $Re<10$, indicative of a laminar regime for a mixing process. The flow of such fluids then obeys the steady-state Stokes equations, that is Equation (1) without the acceleration and inertia terms.

The computational domain was discretized into 290 336 tetrahedra using I-DEAS (EDS) (Figure 5). Solutions of the steady-state Stokes problem obtained with the standard finite element method and the discontinuous pressure $P_1^+-P_0$ element will be used for comparison purposes. Table II gives the characteristics of the meshes generated for both the MINI and the $P_1^+-P_0$ elements. Note that care was taken so that these meshes were fine enough to yield mesh-independent results. A special non-uniform meshing strategy was required for modelling in a suitable way the small clearance between the vessel wall and the impeller. More precisely, a fine mesh was generated close to the bottom gap region between the impeller and the tank walls where the highest shear rates are found. A coarser mesh was used elsewhere. It can be noticed that, in the case of MINI element, the number of equations, after static condensation of the velocity degrees of freedom located at the centroid of each finite element, is approximately one order of magnitude smaller than that with the $P_1^+-P_0$ element.

Simulations were performed on an IBM p690 computer and power draw values were computed from the velocity fields obtained using (19). Figure 6 compares the numerical power curves obtained

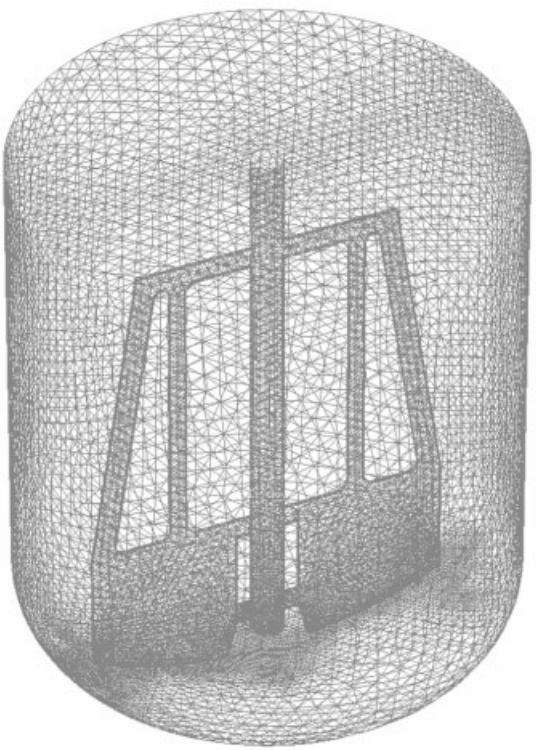

Figure 5. Mesh of the Maxblend impeller system in an unbaffled configuration.

DOI: 10.1002/fld

Table II. Characteristics of the meshes generated for the Maxblend impeller system in an unbaffled configuration.

Finite element	Number of elements	Number of nodes	Number of equations
$P_1^+-P_1$ (MINI)	290 336	346 193	0.2M
$P_1^+-P_0$	290 336	941 549	2.12M

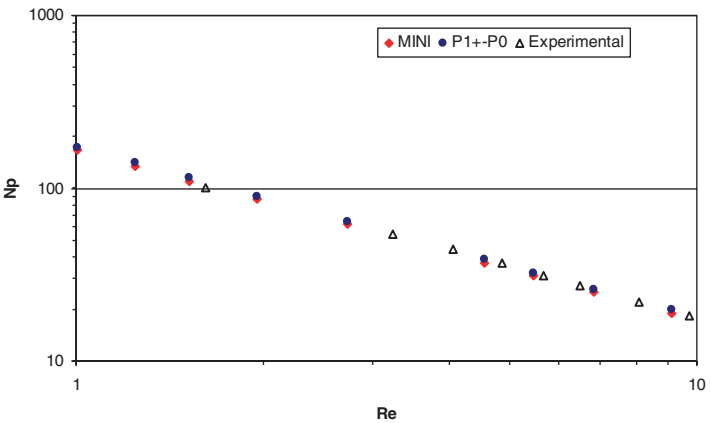

Figure 6. Numerical and experimental power curves for the Maxblend impeller system in an unbaffled configuration.

Table III. Simulation results for the Maxblend impeller system in an unbaffled configuration.

Type of results	Average CPU time (min)	K_p	Discrepancy with respect to the experimental K_p (%)
Experimental	—	180	—
$P_1^+-P_0$	120	176	2
$P_1^+-P_1$ (MINI)	6	170	6

with the $P_1^+-P_0$ and MINI elements to the experimental data of Fradette *et al.* [24]. First, it can be readily noticed that each numerical power curve is in good agreement with the experimental data. These results also comply with the mixing theory, which states that, in the laminar regime ($Re<10$), the power curve exhibits a slope of -1 on a log–log scale. Next, the numerical K_p values computed are 170 and 176 with the MINI and $P_1^+-P_0$ elements, respectively, which are very close to the value of 180 obtained experimentally. These results are summarized in Table III that also gives the average CPU time for the simulations. These CPU times indicate that the MINI element is 20 times faster than the discontinuous pressure $P_1^+-P_0$ element for an almost equivalent accuracy, which makes it very attractive for industrial applications.

DOI: 10.1002/fld

The accuracy of the MINI-based VFEM is next studied. For this purpose, four baffles were added to the Maxblend mixer described above, which renders the fluid flow problem unsteady and forces the use of the VFEM to avoid the need for repetitive remeshings. A Lagrangian frame of reference, that of the impeller, was used, meaning that the baffles are in motion. Viscous fluids identical to those described in the previous case were considered, the flow of which is laminar and obeys the time-dependent Stokes equations, that is, Equation (1) without the inertia term.

The corresponding boundary conditions were as follows:

1. a no-slip condition on the Maxblend impeller;
2. the rotational speed ω on the baffles;
3. the rotational speed ω on the vessel walls;
4. the surface is considered flat.

The fluid was supposed at rest at $t=0$. From a numerical standpoint, the mesh generated previously for the unbaffled configuration was used here in the VFEM to represent the vessel and the impeller. A set of 6432 control points was generated using I-DEAS (EDS) to take into account the four baffles (Figure 7). Note that the number of control points was adjusted with respect to the number

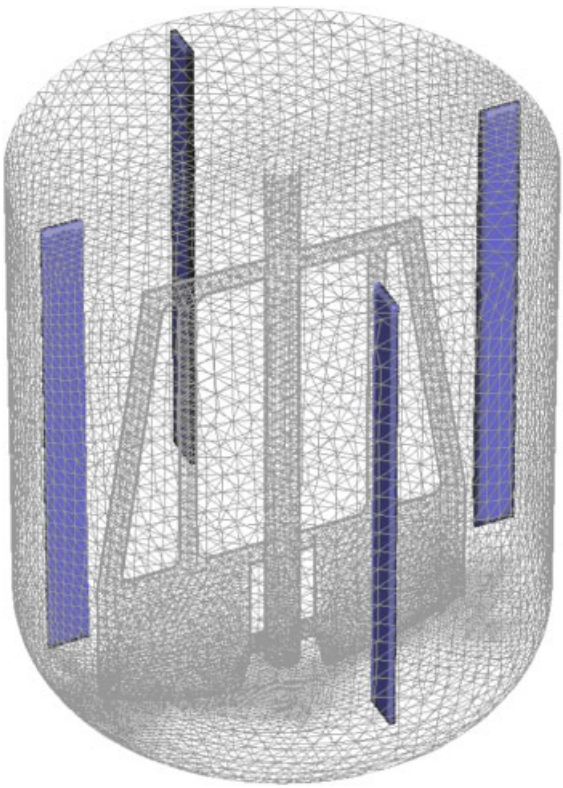

Figure 7. Mesh of the Maxblend impeller system in a baffled configuration.

DOI: 10.1002/fld

of finite elements, as explained in Bertrand *et al*. [2] and assessed by Rivera *et al*. [28], so that the resulting problem does not become overconstrained.

The value of the time step for a simulation with the VFEM is known to affect the accuracy of the solution and the stability of the model. For more details about this point, we refer the reader to Iranshahi *et al*. [29]. In practice, a trade-off between CPU time and accuracy must be sought. Here, the time step was set to 0.1s. Each simulation was performed for three full revolutions (60 time steps). Table IV summarizes the CPU time required for a transient simulation with the VFEM. Results in the case of the MINI element refer to the VFEM and the fully coupled solver, whereas those for the discontinuous pressure $P_1^+-P_0$ element were obtained with the VFEM and the decoupled approach. As can be seen, the MINI-based VFEM introduced in this work outperforms the $P_1^+-P_0$/VFEM combination in terms of CPU time by a factor of 30.

As for accuracy, Figure 8 compares the numerical power curves to the experimental data of Fradette *et al.* [24]. The experimental K_p value is 218. As in the previous case, each power curve exhibits a slope of -1 on a log–log scale in the laminar regime ($Re<10$). The numerical K_p values computed with the MINI and the $P_1^+-P_0$ elements are 194 and 198, respectively. This

Table IV. Simulation results for the Maxblend impeller system a baffled configuration.

Type of results	Average CPU time per time step (min)	Total CPU time	K_p	Discrepancy with respect to the experimental K_p (%)
Experimental	—	—	218	—
$P_1^+-P_0$ decoupled approach	60	$2\frac{1}{2}$ days	198	9
$P_1^+-P_1$ (MINI) fully coupled approach	2	2 h	194	11

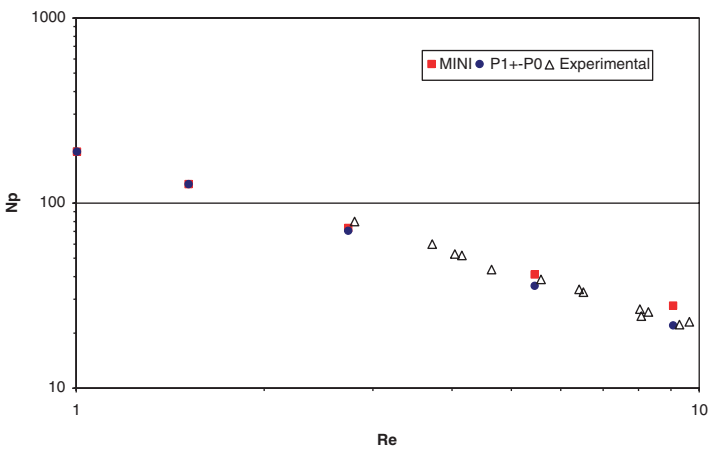

Figure 8. Numerical and experimental power curves for the Maxblend impeller system in a baffled configuration.

DOI: 10.1002/fld

corresponds to a similar discrepancy of around 10% in both cases. In particular, it shows again the efficiency of the MINI-based VFEM for the simulation of viscous fluid flow in industrial mixing applications.

6. INDUSTRIAL FLOW IN A THREE-BLADE PLANETARY MIXER

The new MINI-based VFEM was next applied to the industrial case of the laminar flow of a propellant-type highly viscous fluid in a three-blade planetary mixer. Planetary mixers are known to provide a suitable bulk circulation and good homogenization for this type of fluid. Besides, owing to their close-clearance nature, their scraping action leads to an efficient transfer of the paste located at the periphery to the vessel bulk.

The three-blade planetary mixer is presented in Figure 9. It consists of a steel vessel of 50 US gallons (around 200 l), two external scraping arms (twin-blade impeller) and one centered scraping arm (four-blade impeller). The tank has a diameter of 0.53 m and a height of 0.24 m. The three arms are mounted on a rotating carrousel, which guarantees that the whole volume of the vessel is swept within one single revolution of the carrousel. The lateral surface of the mixer blades is helical thus ensuring good pumping capability.

In this work, the two external impellers rotated counterclockwise at 30 rpm. The central impeller rotated clockwise at 15 rpm. The rotational speed of the carrousel was set to 5 rpm. The speed ratios between the external impellers and the central impeller, and between the central impeller and the carrousel were equal to 2 and 3, respectively, which conforms to the design specifications.

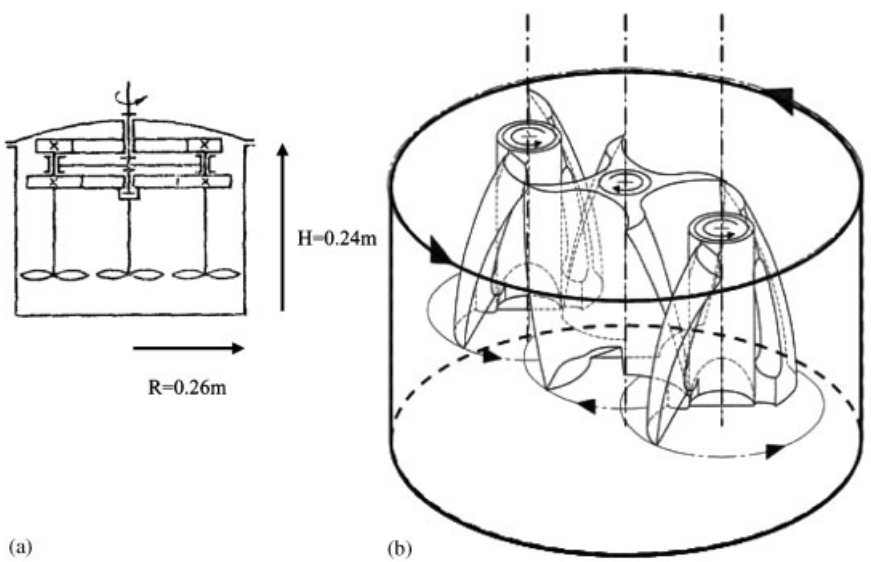

Figure 9. (a) Three-blade planetary mixer with the blades on off-centered shafts and a central wheel shaft (adapted from Kol'man-Ivanov and Shklovskaya [30]) and (b) motion of the blades.

DOI: 10.1002/fld

For the sake of completeness, Figure 10 shows the top view of the central impeller and one of the two external impellers.

Solid rocket propellants are thermoset composite materials consisting of a ground oxidizer dispersed into a rubbery matrix. Polypropylene glycol (PEG) and hydroxyl-terminated polybutadiene (HTPB) are the most frequent elastomer matrices. The blend is cross-linked by means of a curing agent such as hexamethylene diisocyanate (HMDI). Rheological measurements have shown that this type of paste exhibits a slight shear-thinning behavior so that, in practice, it can be modelled as a Newtonian viscous fluid [7].

The paste considered in this study had a density ρ of $1800\,\mathrm{kg/m^3}$ and a viscosity μ of $400\,\mathrm{Pa\,s}$, typical of a propellant at the end of the kneading cycle in a planetary mixer. The flow of such fluid under the operating conditions described above is laminar and is governed by the unsteady Stokes equations.

The results obtained with the MINI-based VFEM and both the coupled and decoupled approaches of Sections 3.2 and 3.1, respectively, will be compared with those obtained with the P_1^+–P_0/VFEM combination of Bertrand *et al.* [2] for which only the decoupled approach was used.

The computational domain was discretized into tetrahedra using I-DEAS (EDS). The clearance between the external blades and the vessel wall is very small so that the highest shear rates

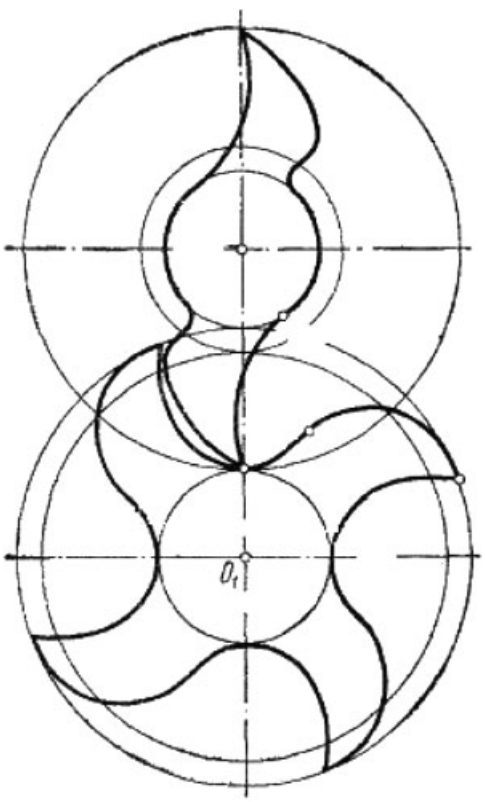

Figure 10. Top view of the central impeller and one of the two external impellers (adapted from Kol'man-Ivanov and Shklovskaya [30]).

DOI: 10.1002/fld

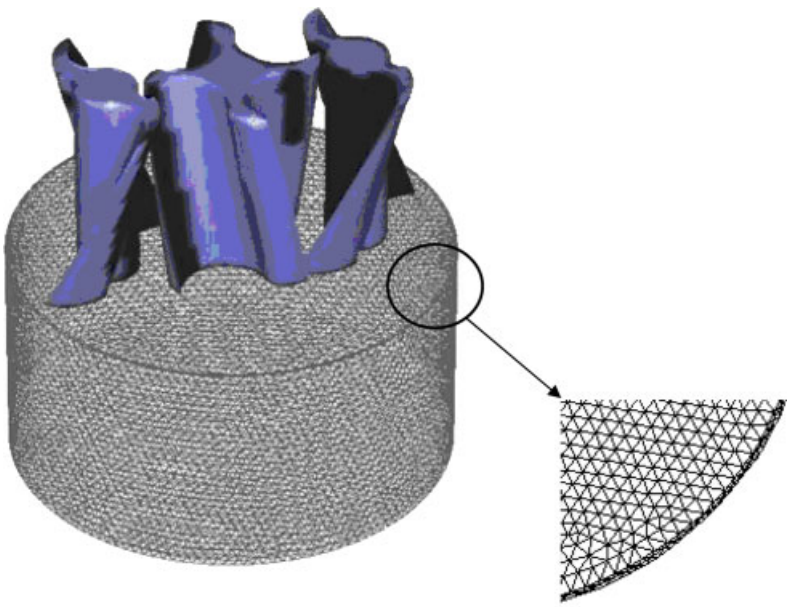

Figure 11. Mesh for the three-blade planetary mixer.

Table V. Characteristics of the meshes generated for the three-blade planetary mixer.

Finite element	Number of elements	Number of nodes	Number of equations
P_1^+–P_1 (MINI)	169 882	202 115	0.1M
P_1^+–P_0	169 882	549 340	1.26M

are expected to occur in these gaps. Consequently, a smaller mesh size was chosen for these regions.

The mesh generated, which is shown in Figure 11, contains 169 882 elements. The corresponding numbers of nodes and equations can be found in Table V for both the MINI and the P_1^+–P_0 elements. All three impellers were taken into account by means of a total of 5507 control points. This number was adjusted with respect to the number of finite elements in the static mesh so that the problem is not overconstrained but that the distance between any two control points is small enough to prevent fluid from penetrating into the blades. Initially, the fluid was assumed at rest. A time step of 0.6 s was set for the transient simulations. This value ensures that one of the time steps corresponds to the smallest blade/wall gap. The motion of the three blades of the planetary mixer is symmetric and the flow inside is periodic. All the simulations were performed for a half revolution of the carrousel only, which corresponds to 10 time steps, to show that the proposed coupled approach works.

Figures 12 and 13 display, respectively, the norm of the velocity field at the third and seventh time steps on three different cross sections, for the MINI and the P_1^+–P_0 elements. These two

DOI: 10.1002/fld

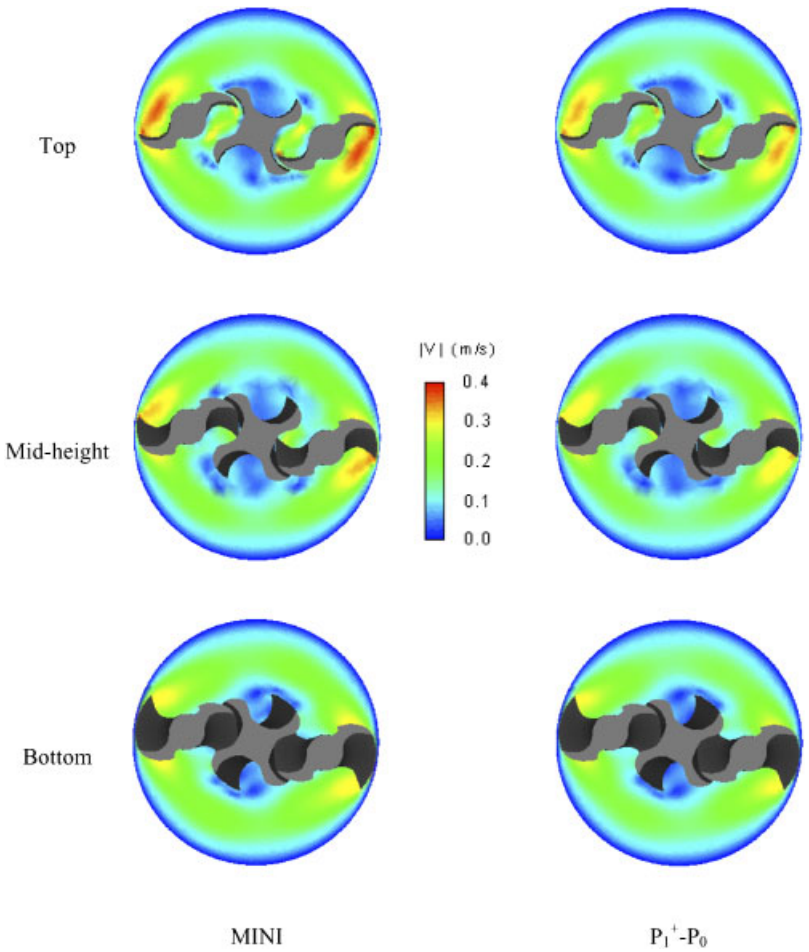

Figure 12. Norm of the velocity field at the third time step on three different cross sections.

time steps correspond to positions of the kneading blades where the clearance to the vessel wall is the lowest (third) and the highest (seventh). Generally speaking, a good agreement can be noticed for these two time steps. In fact, a closer investigation reveals that the MINI element slightly overestimates with respect to the $P_1^+ - P_0$ element (by around 5%) the maximum of this scalar field. In particular, one may notice, for the MINI element only, the presence of a peak between the central blade and one of the external blades. These figures also show that the three-blade planetary mixer exhibits good scraping capability on all three cross sections, as evidenced by the higher velocity gradients found in neighborhood of the blades and in the area between the external blades and the central blade.

Figures 14 and 15 display, respectively, the axial component of the velocity field (w) of the mixer at the third and seventh time steps on the mid-height cross section. A good agreement between both elements can be noticed although the MINI element seems to predict larger

DOI: 10.1002/fld

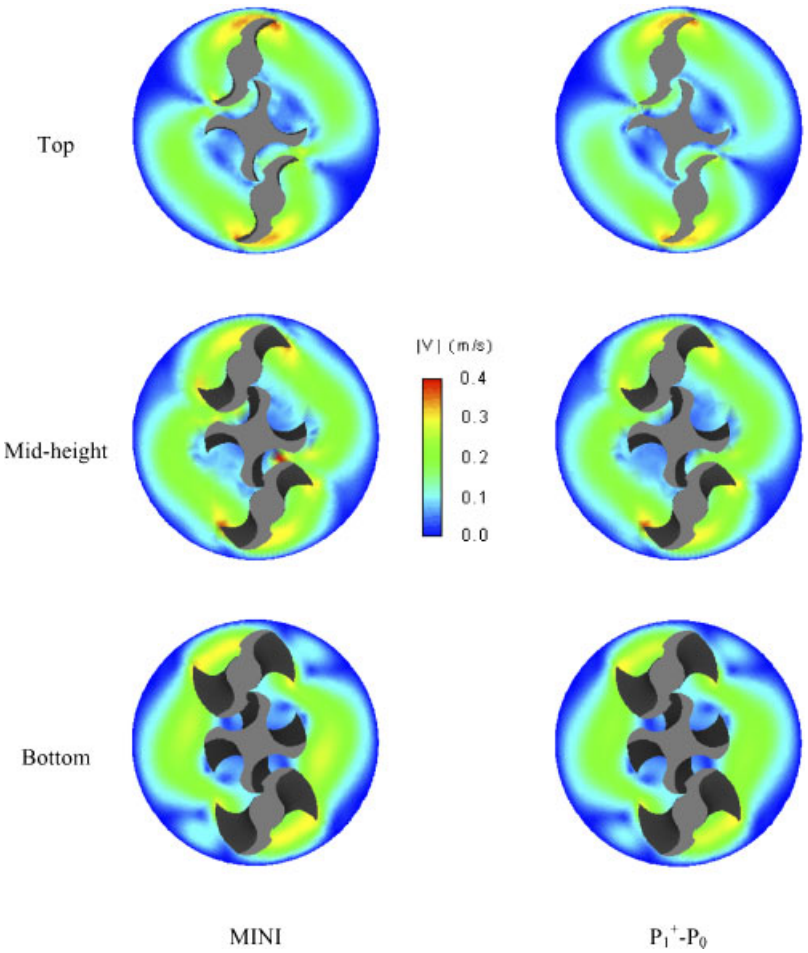

Figure 13. Norm of the velocity field at the seventh time step on three different cross sections.

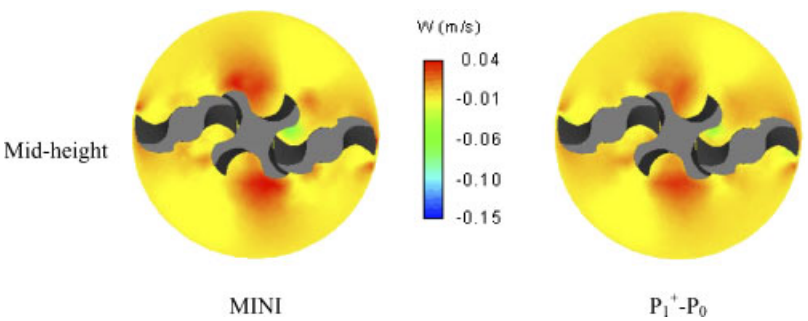

Figure 14. Axial component of the velocity field at the third time step on the mid-height cross section.

DOI: 10.1002/fld

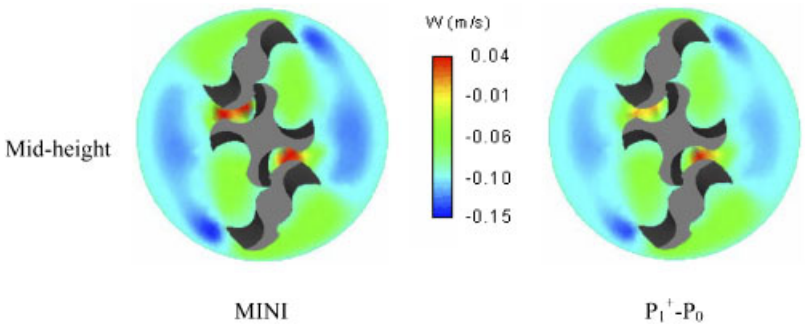

Figure 15. Axial component of the velocity field at the seventh time step on the mid-height cross section.

values of the axial component of the velocity in some areas. Owing to the high viscosity of the paste, efficient pumping is found, as expected, in rather small areas located near the impellers. The motion of the helical blades compresses the paste in these zones, which is then pumped upward.

Figures 16 and 17 show the shear stress (*xy*-component of the stress tensor) on the mid-height cross section for both elements at the third and seventh time steps, respectively. Here again, a good agreement between the MINI and the $P_1^+ - P_0$ elements can be observed. As expected, the maximum shear stress is found where the clearance value with the wall is the lowest. Moreover, the maximum obtained at the third time step is higher than that at the seventh time step, which is due to a smaller blade/wall gap in the former case. This point emphasizes the importance of having a mesh with enough elements in the gap region between the blades and the wall to obtain an accurate solution. A zone of high shear stress can also be noticed in the center of the bulk, more precisely in the clearance between the internal and the external blades.

The power consumption was computed through a macroscopic energy balance following (19). Figure 18 shows how the power draw varies over a half period of the carrousel. A particularity of planetary mixers is that the clearance between the blades and the vessel wall is a periodic function of time. Given that the volume average shear stress is itself a function of the blades-to-wall distance, the power consumption is also time dependent. One may notice that the power curves obtained with the MINI and the $P_1^+ - P_0$ elements are very close, with a relative difference smaller than 10%.

The CPU time required for each transient simulation is presented in Table VI. It can be seen that the MINI-based VFEM with the fully coupled approach is 7 times faster than with the decoupled approach, and that this former strategy outperforms the $P_1^+ - P_0$/VFEM combination with the decoupled approach by a factor of more than 100!

7. CONCLUSION

The objective of this work was to develop a fast three-dimensional numerical strategy for the simulation of viscous fluid flow in complex mixing systems. The method that was introduced is based on the virtual finite element method (VFEM) of Bertrand *et al*. [2] and the inexpensive MINI finite element. Two methods were also discussed for the solution of the underlying partial

DOI: 10.1002/fld

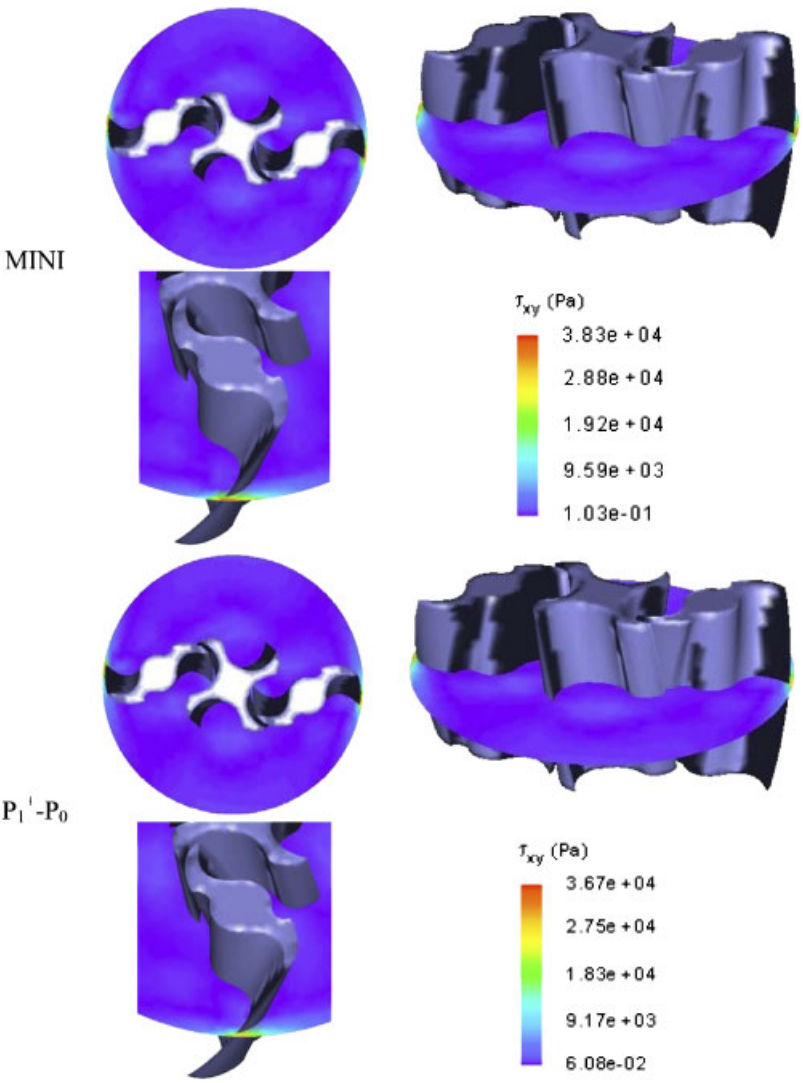

Figure 16. Shear stress on the mid-height cross section at the third time step.

differential equations: (i) a decoupled approach wherein the velocity and the pressure are solved for in a coupled manner through a penalty technique, and the Lagrange multiplier is obtained as in Bertrand *et al.* [2] through the Uzawa algorithm, and (ii) a fully coupled approach that solves for the velocity, the pressure and the Lagrange multiplier associated with the kinematics constraints in a fully coupled manner by means of a consistent penalty technique. The accuracy of the MINI-based VFEM was tested successfully against experimental data in the case of a Maxblend impeller system. A comparison was also made with the P_1^+–P_0/VFEM combination of Bertrand *et al.* [2]. Our new technique was then applied to the simulation of the flow of a Newtonian

DOI: 10.1002/fld

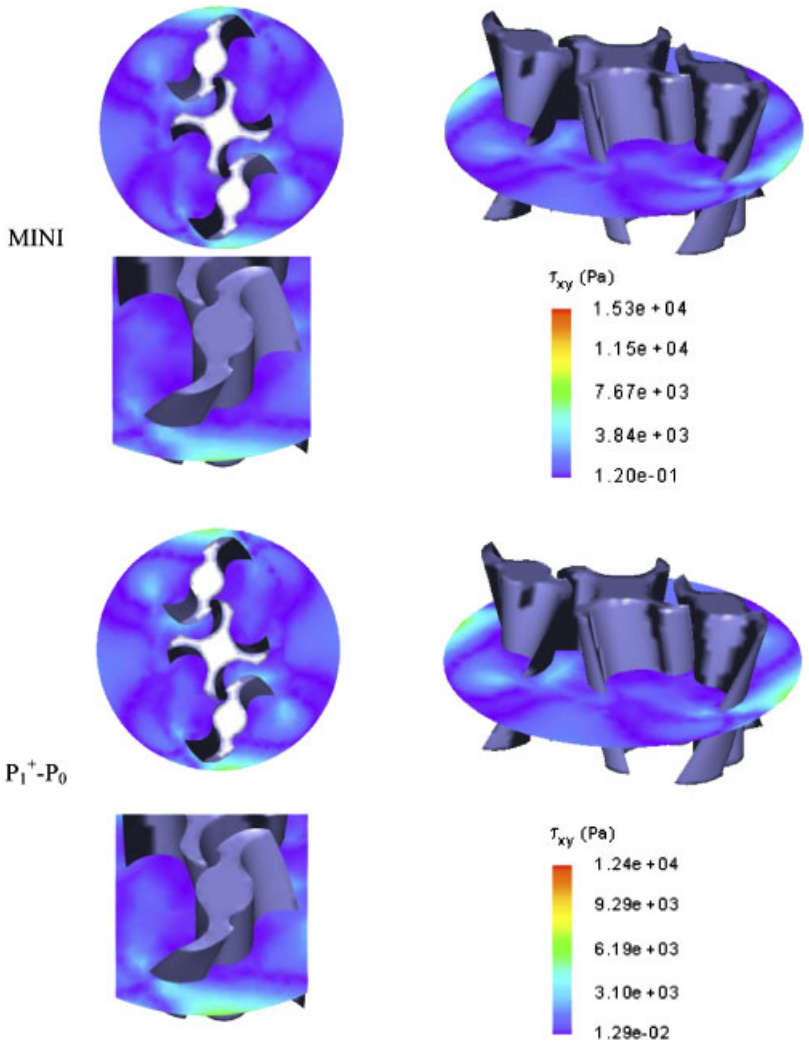

Figure 17. Shear stress on the mid-height cross section at the seventh time step.

viscous fluid in a three-blade planetary mixer. The results obtained show that the MINI-based VFEM is a suitable strategy for simulating the flow of viscous fluids in complex mixing systems since its accuracy is comparable with that obtained with the P_1^+–P_0/VFEM at a fraction of the cost.

Finally, preliminary results (not shown in this paper) in the case of the Maxblend impeller system have revealed that the accuracy of the MINI-based VFEM tends to decrease when the Reynolds number is increased above 10, that is outside of the laminar regime. Two possible causes for this are the use of penalization and ill-conditioning of the corresponding global matrix (e.g. Pelletier *et al*. [19]), or some locking phenomena, as previously observed in the case of low-order

DOI: 10.1002/fld

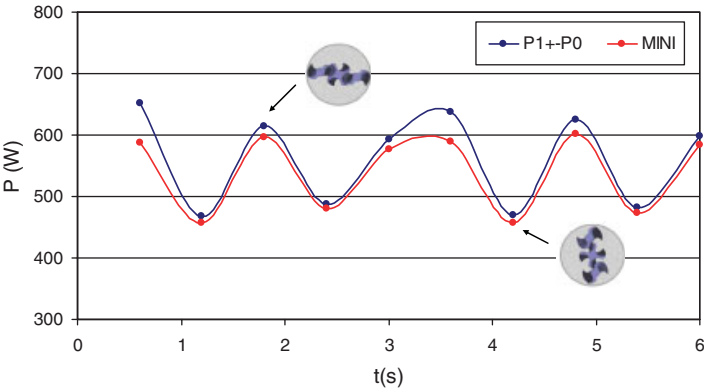

Figure 18. Power consumption of the three-blade planetary mixer.

Table VI. CPU time for the three-blade planetary mixer.

Finite element	Average CPU time per time step (min)	Total CPU time
MINI-based VFEM+coupled approach	4.5	45 min
MINI-based VFEM+decoupled approach	30	5 h
P_1^+–P_0/VFEM+decoupled approach	504	$3\frac{1}{2}$ days

finite elements when a penalty technique is used (e.g. Bercovier [31]). This will be the topic of future work.

ACKNOWLEDGEMENTS

The authors would like to acknowledge the financial contribution of the National Science and Engineering Research Council of Canada (NSERC) and the Fond Québecois de la Recherche sur la Nature et les Technologies (FQRNT).

REFERENCES

1. Tanguy PA, Thibault F, Dubois C, Aït-Kadi A. Mixing hydrodynamics in a double planetary mixer. *Chemical Engineering Research and Design* 1999; **77**(A4):318–324.
2. Bertrand F, Tanguy PA, Thibault F. A three-dimensional fictitious method for incompressible fluid flow problems. *International Journal for Numerical Methods in Fluids* 1997; **25**:719–736.
3. Glowinski R, Pan T, Périaux J. A fictitious domain method for Dirichlet problem and applications. *Computer Methods in Applied Mechanics and Engineering* 1994; **111**(3–4):283–303.
4. Bertrand F, Thibault F, Tanguy PA, Choplin L. 3D modelling of highly viscous polymers with intermeshing impellers. In *Process Mixing—Chemical and Biochemical Applications*, Tatterson G, Calabrese R (eds). AIChE Symposium Series, vol. 299, American Institute of Chemical Engineers: New York, 1994; 106–116.
5. Tanguy PA, Bertrand F, Labrie R, Brito-De-La-Fuente E, Fages MH. Étude numérique du malaxage de fluides chargés dans un malaxeur bipale à mouvement planétaire. *Récents Progrès en Génie des Procédés* (Lavoisier TecDoc) 1995; **38**:87–92.

DOI: 10.1002/fld

6. Tanguy PA, Bertrand F, Labrie R, Brito-De-La-Fuente E. Numerical modelling of the mixing of viscoplastic slurries in a twin-blade planetary mixer. *Chemical Engineering Research and Design* 1996; **74**(A4):499–504.
7. Tanguy PA, Bertrand F, Thibault F, Fages F, Lamotte M, Giraud E, Fages MH. Mécanismes de malaxage dans un malaxeur bipale à mouvement planétaire: simulation numérique 3D et étude expérimentale par traçage fluorimétrique. *Récents Progrès en Génie des Procédés* 1998; **61**:43–48.
8. Jongen T. Characterization of batch mixers using numerical flow simulations. *AIChE Journal* 2000; **46**(11): 2140–2150.
9. Jongen T, Bruschke MV, Dekker JG. Analysis of dough kneaders using numerical flow simulations. *Cereal Chemistry* 2003; **80**(4):383–389.
10. Avalosse TH, Crochet MJ. Finite-element simulation of mixing: 1. Two-dimensional flow in periodic geometry. *AIChE Journal* 1997; **43**(3):577–587.
11. Avalosse TH, Rubin Y, Fondin L. Non-isothermal modeling of co-rotating and contra-rotating twin screw extruders. *Journal of Reinforced Plastics and Composites* 2002; **21**(5):419–429.
12. Connelly RK, Kokini JL. Mixing simulation of a viscous Newtonian liquid in a twin sigma blade mixer. *AIChE Journal* 2006; **52**(10):3383–3393.
13. Gartling DK. Multipoint constraint methods for moving body and non-contiguous mesh simulations. *International Journal for Numerical Methods in Fluids* 2005; **47**:471–489.
14. Clifford MJ, Cox SM, Finn MD. Reynolds number effects in a simple planetary mixer. *Chemical Engineering Science* 2004; **59**:3371–3379.
15. Delaplace G, Guérin R, Leuliet JC. Dimensional analysis for planetary mixer: modified power and Reynolds numbers. *AIChE Journal* 2005; **51**(12):3094–3100.
16. Delaplace G, Thakur RK, Bouvier L, André C, Torrez C. Dimensional analysis for planetary mixer: mixing time and Reynolds numbers. *Chemical Engineering Science* 2007; **62**:1442–1447.
17. Arnold DN, Brezzi F, Fortin M. A stable finite element for Stokes equations. *Calcolo* 1984; **21**:337–344.
18. Reddy JN. On penalty function methods in the finite-element analysis of flow problems. *International Journal for Numerical Methods in Fluids* 1982; **2**:151–171.
19. Pelletier D, Fortin A, Camarero R. Are FEM solutions of incompressible flows really incompressible? (Or how simple flows can cause headaches!). *International Journal for Numerical Methods in Fluids* 1989; **9**:99–112.
20. Langtangen HP, Mardal K, Winther R. Numerical methods for incompressible viscous flow. *Advances in Water Resources* 2002; **25**:1125–1146.
21. Rivera C, Foucault S, Heniche M, Espinosa-Solares T, Tanguy PA. Mixing analysis in a coaxial mixer. *Chemical Engineering Science* 2006; **61**:2895–2907.
22. Barailler F, Heniche M, Tanguy PA. CFD analysis of a rotor–stator mixer with viscous fluids. *Chemical Engineering Science* 2006; **61**:2888–2894.
23. Paul EL, Atiemo-Obeng VA, Kresta SM. *Handbook of Industrial Mixing*, *Science and Practice*. Wiley/Interscience: New York, 2004.
24. Fradette L, Thomé G, Tanguy PA, Takenaka K. Power and mixing time study involving a Maxblend impeller with viscous Newtonian and non-Newtonian fluids. *Chemical Engineering Research and Design* 2007; **85**(A11): 1514–1523. DOI: 10.1205/cherd07051.
25. Iranshahi I, Devals C, Heniche M, Fradette L, Tanguy PA, Takenaka K. Hydrodynamics characterization of the Maxblend impeller. *Chemical Engineering Science* 2007; **62**:3641–3653.
26. Bertrand F, Gadbois M, Tanguy PA. Tetrahedral elements for fluid flow problems. *International Journal for Numerical Methods in Engineering* 1992; **33**:1251–1267.
27. Tanguy PA, Lacroix R, Bertrand F, Choplin L, Brito-De-La-Fuente E. Finite element analysis of viscous mixing in a helical ribbon screw impeller. *AIChE Journal* 1992; **38**(6):939–944.
28. Rivera C, Heniche M, Ascanio G, Tanguy PA. A virtual finite element model for centered and eccentric mixer configurations. *Computers and Chemical Engineering* 2004; **28**:2459–2468.
29. Iranshahi I, Heniche M, Bertrand F, Tanguy PA. Numerical investigation of the mixing efficiency of the Ekato Paravisc impeller. *Chemical Engineering Science* 2006; **61**:2609–2617.
30. Kol'man-Ivanov EE, Shklovskaya FA. Geometric design of planetary mixers where the blades clean one another. Translated from *Khimicheskoe i Neftyanoe Machinostroenie* 1966; **3**:14–20.
31. Bercovier M. Perturbation of mixed variational problems. Applications to mixed finite element methods. *RAIRO Analyse Numérique* 1978; **12**:211–236.